



ELSEVIER

Journal of Crystal Growth 169 (1996) 51–60

JOURNAL OF **CRYSTAL
GROWTH**

CH₃I vapor etching of GaAs in a vertical rotating-disk reactor

C.W. Krueger^{a,b,*}, S. Patnaik^a, C.A. Wang^b, M. Flytzani-Stephanopoulos^{a,1}

^a Department of Chemical Engineering, Massachusetts Institute of Technology, Cambridge, Massachusetts 02139, USA

^b Lincoln Laboratory, Massachusetts Institute of Technology, Lexington, Massachusetts 02173-9108, USA

Received 11 October 1995; accepted 4 March 1996

Abstract

A detailed computer model which predicts etch rates and spatial uniformity for chemical vapor etching of GaAs with CH₃I in a vertical rotating-disk organometallic vapor phase epitaxy (OMVPE) reactor has been developed. Etch rate predictions compare favorably with experiments performed in the vertical reactor at several temperatures ranging from 525 to 590°C and CH₃I mole fractions from 0.005 to 0.050 in an H₂ carrier gas. Agreement between the data and the model verifies our earlier assertion that gas phase decomposition of CH₃I is the rate-limiting step, and that the etchant species are I and to a lesser extent CH₃ radicals. Predictions further show that radial etch rate uniformity improves from a 5% variation over 50% of the substrate at low rotation (20–100 rpm) to a 5% variation over 80% of the substrate at 500 rpm. Increasing rotation rate also reduces the etch rate, a result that is in contrast to earlier results for OMVPE growth from TMGa and AsH₃. These contrasting results arise because growth is rate limited by gas phase diffusion of TMGa, whereas CH₃I vapor etching is rate limited by gas phase decomposition of CH₃I.

1. Introduction

Chemical vapor etching of semiconductor materials is a potentially valuable process for in situ use in organometallic vapor phase epitaxy (OMVPE). With a viable in situ etch complementing epitaxial growth, OMVPE could be more conveniently applied to the fabrication of nonplanar GaAs/AlGaAs devices for which ex situ etching would lead to aluminum oxidation and a subsequent lowering of device performance. In our previously reported studies of vapor

etching of GaAs and AlGaAs by CH₃I, it was shown that (100)GaAs and AlGaAs could be etched smoothly at temperatures below 500°C, which is lower than for most previously studied vapor etches [1]. Furthermore, (100)GaAs surfaces etched by this process were suitable for OMVPE growth of high quality GaAs [2].

In this paper, a detailed model for CH₃I vapor etching in a vertical rotating-disk reactor is presented. The model is based on a previous one for this reactor [3], and has been extended to include CH₃I/H₂ gas phase reaction chemistry and radiative heat transfer. The reactor has the main advantage that deposition can be achieved with a high degree of radial uniformity through adjustment of the

* Corresponding author.

¹ Present address: Department of Chemical Engineering, Tufts University, Medford, Massachusetts 02155, USA.

disk rotation rate. Favorable comparison between the etch rates predicted by this model and those measured experimentally validates the model and further supports our previous assertion that the etch rate is controlled by gas phase decomposition of CH_3I [1].

2. Model formulation

A schematic of the vertical rotating-disk reactor system is shown in Fig. 1, and the specific details of this design have been described elsewhere [4]. The main characteristic dimensions are a 10 cm tube diameter, a 6.7 cm susceptor diameter, and a 15 cm inlet-to-susceptor distance. Details of the numerical model formulation [3] are summarized here. The model is a finite-element representation of the reactor in two dimensions assuming axial symmetry, and includes the equations for momentum, energy, and mass transport. The approach used to perform the calculations takes advantage of the fact that the reactant (CH_3I) is present in only dilute amounts

(0.005–0.05 mole fraction) with most of the gas being H_2 . This allows heat of chemical reaction effects to be ignored and velocity/temperature calculations to be decoupled from reaction/mass transfer computation. In practice, the velocity and temperature fields are first computed and serve as inputs to a separate reaction/mass-transfer model. The current developments of this model have incorporated effects of radiative heat transfer on the computed temperature field and the mass transfer equations have been extended to handle multi-component systems with gas phase chemical reaction. Surface consumption rates of etchant species are treated in a probabilistic fashion through the use of reactive sticking coefficients.

2.1. Flow and temperature equations

The following equations are used to describe the flow and temperature fields in the vertical rotating-disk reactor.

Conservation of momentum:

$$\rho \mathbf{v} \cdot \nabla \mathbf{v} = -\nabla p + \nabla \cdot (\mu \dot{\gamma}) - \frac{2}{3} \nabla [\mu (\nabla \cdot \mathbf{v})] - g \rho \mathbf{e}_z, \quad (1)$$

where ρ is the gas density, \mathbf{v} is the velocity vector, p is the pressure, μ is the gas viscosity, $\dot{\gamma}$ is the rate of strain tensor, g is the gravitational constant, and \mathbf{e}_z is the unit vector in the z -direction.

Conservation of mass:

$$\nabla \cdot (\rho \mathbf{v}) = 0. \quad (2)$$

Equation of state:

$$\rho = pM/R_G T, \quad (3)$$

where M is the average molecular weight of the gas and R_G is the gas constant.

Conservation of energy:

$$\text{gas: } \rho C_p \mathbf{v} \cdot \nabla T = \mathbf{v} \cdot \nabla p + \nabla \cdot (k_g \nabla T), \quad (4)$$

$$\text{wall: } \nabla \cdot (k_w \nabla T_w = 0), \quad (5)$$

where C_p is the gas heat capacity, k_g is the gas thermal conductivity, k_w is the reactor wall thermal conductivity, and T_w is the wall temperature.

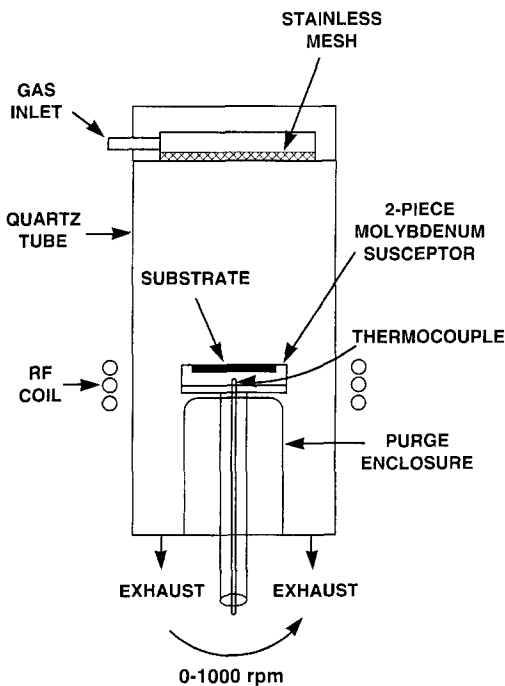


Fig. 1. Schematic of vertical rotating-disk reactor.

Boundary conditions:

$$-k_g \frac{\partial T_k}{\partial r} = -k_w \frac{\partial T_k}{\partial r} + \sigma \epsilon_k \left(T_k^4 - \frac{1}{\epsilon_k A_k} \sum_{j=1}^{N_s} A_j \epsilon_j G_{jk} T_j^4 \right),$$

$$r = R_w, \quad (6)$$

$$-k_w \frac{\partial T}{\partial r} = H_T (T - T_0) + \sigma \epsilon_w (T_w^4 - T_0^4), \quad r = R.$$

$$(7)$$

Eqs. (6) and (7) are the heat transfer boundary conditions at the inside and outside of the reactor tube wall, respectively. H_T is the outer wall heat transfer coefficient which is estimated from standard correlations for free convection around a vertical cylinder, T_0 is the ambient temperature, and σ is the Stefan–Boltzmann constant. Eq. (6) is written for each surface element of the reactor wall (k) where G_{jk} is the Gebhart factor between the surface elements k and j ; T_j , T_k are the temperatures of surface elements j and k ; ϵ_j , ϵ_k are the diffuse gray body emissivities; and A_j , A_k are the surface areas. The N surface elements (j) include all of the internal reactor surfaces. The last term in each of Eqs. (6) and (7) represents heat transfer due to radiation from the reactor inner surfaces to the inner wall and from the outer wall to the ambient, respectively. For these calculations, the quartz tube wall is treated as an opaque, diffuse gray body and the gas inside the reactor is considered to be transparent to radiation. The remaining boundary conditions are the no slip velocity condition at all solid surfaces, the ambient temperature T_0 and the uniform velocity field at the reactor inlet, $\mathbf{v}(r, \vartheta, z) = (0, 0, v_i)$. Finally, the flow and temperature fields are assumed to be fully developed at the reactor outlet.

2.2. Multispecies conservation

For mass transport by convection and diffusion and gas phase chemical reactions, the following species conservation equation is solved for n components in terms of weight fractions (y_i):

$$\rho \left(\frac{\partial y_i}{\partial t} \right) + \rho (\mathbf{v} \cdot \nabla y_i) = \nabla \cdot [D_i \rho \nabla y_i + D_i^T \nabla (\ln T)] + \mathbf{R}_i, \quad (8)$$

where \mathbf{R}_i is the net reaction term for species i (i.e., the net consumption and production of species i from the full set of gas phase chemical reactions considered). D_i is the binary diffusion coefficient and D_i^T is the thermal diffusion coefficient for species i . The dilute species approximation is implicit in this formulation, i.e., the gas density (ρ) is assumed to be independent of y_i .

2.3. Surface reaction boundary condition

The expression for describing finite surface reaction rates \mathbf{R}_{sur} is

$$\mathbf{R}_{\text{sur}(i)} = \frac{\sigma_i y_i \rho R_G T}{\sqrt{2\pi m_i R_G T}}, \quad (9)$$

where σ_i is the surface reaction probability (a value between 0 and 1) which is multiplied by the surface collision frequency for species i , a result derived from kinetic theory where m_i is the molar mass of species i and R_G is the ideal gas constant. The values for the σ_i are unknown and, depending on the exact nature of the surface reaction kinetics, may have complex dependencies on variables such as surface temperature and coverage. In these calculations it is usually assumed that $\sigma_i = 1$ for etchant species, resulting in an upper bound prediction for etch rates. In addition, the effect of varying σ_i between 0 and 1 has been examined. The surface boundary condition for each component (i) is obtained by balancing Eq. (9) to the gas phase supplied flux to the reacting surface:

$$D_i \rho \frac{\partial y_i}{\partial z} + D_i^T \frac{\partial (\ln T)}{\partial z} = \mathbf{R}_{\text{sur}(i)}. \quad (10)$$

It is important to note that desorbing products are not accounted for in this formulation. In other words, adsorbed species are simply considered to disappear at the surface according to the kinetics described above. Etch rate is computed from the solid density of GaAs and the surface reaction stoichiometry. For the present application of this model to describe CH_3I vapor etching, this approximation will be valid since gas phase reactions are expected to be rate controlling. A failure of this assumption will be evident if the predicted etch rates are substantially higher than experimental values.

2.4. Computational details

Eqs. (1)–(10) are solved using standard Galerkin finite-element methods. A 20×80 computational domain is shown in Fig. 2 and consists of rectangular elements. The mesh is refined near the reactor inlet and at the susceptor boundaries. Above the susceptor, successive geometric refinements in the z -direction are used as this is where the sharpest concentration gradients are expected to be encountered. The reactor wall is represented by the two outer elements in the radial direction. Velocity, temperature, and concentration fields are represented by biquadratic polynomials and the pressure field by bilinear polynomials.

Gas viscosity, heat capacity, and thermal conductivity are assumed to be those for pure hydrogen. The binary species diffusion coefficients (D_i , for species i in hydrogen) used in these calculations are estimated using standard methods and account for temperature and pressure dependences. Values for thermal diffusion coefficients and their temperature dependences are estimated using the technique re-

ported by Holstein [5]. Gray body emissivities were assumed to be 0.1 for the molybdenum susceptor, 0.3 for the stainless steel inlet, and 0.8 for the quartz walls. The emissivity of the GaAs wafer which was present on top of the molybdenum susceptor during the etch experiments described in Section 3 has been neglected since only small wafers (1×1 cm) were used.

3. Experimental procedure

Two types of experiments were performed using the vertical rotating-disk reactor for purposes of comparison with model predictions. The first were measurements of the external reactor wall temperature under nonreacting conditions in order to independently verify the heat transfer component of the model. The second were measurements of etch rates of GaAs by $\text{CH}_3\text{I}/\text{H}_2$ as a function of temperature and CH_3I concentration.

For measuring external wall temperatures, a chromel–alumel thermocouple junction was directly contacted with the outer reactor wall and held in place by a thin quartz rod. The thermocouple junction itself was formed by welding the ends of chromel and alumel wire into a bead which was then flattened out. With this arrangement, conduction of heat away from the junction is not expected to be significant. The susceptor temperature was measured by a thermocouple inserted into the bottom of the molybdenum susceptor. Etch/growth temperatures had been previously verified to be accurate by comparison to surface optical pyrometer measurements [4]. During these experiments, a constant flow of hydrogen to the reactor was maintained at 10 slpm, the reactor pressure was 0.2 atm, and the disk was rotated at 450 rpm. Wall temperature measurements were taken at several different positions above the top of the susceptor. The susceptor temperature was varied from 500 to 800°C.

The CH_3I vapor etching experiments in the vertical rotating-disk reactor were performed under the following conditions. The total hydrogen flow to the reactor was 10 slpm, the reactor pressure was 0.2 atm, and the susceptor was rotated at 20 rpm. These operating conditions assure that the flow is laminar and free from any convection-driven recirculation

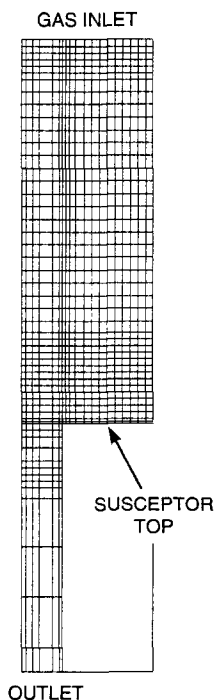


Fig. 2. Finite-element mesh used for calculations.

[6]. The etch temperature ranged from 525 to 590°C, and CH₃I concentrations from 0.005 to 0.05 mol fraction. The substrates were GaAs epilayers which were previously grown by OMVPE over a thin Al_{0.4}Ga_{0.6}As marker layer on a GaAs substrate. Etch depths were determined by comparing the remaining GaAs epilayer thickness to the original value. Epilayer thicknesses were measured with a mechanical stylus after removing a portion of the remaining GaAs epilayer by masking and selectively etching the unmasked GaAs down to the AlGaAs marker.

4. Verification of extended heat transfer model

Since temperature and velocity fields are computed independently of the mass transfer and chemical reactions, temperature field computations were experimentally verified. In a previous study in a horizontal OMVPE reactor, verification was done directly by comparing model predictions to internal hydrogen gas temperatures which were measured by 2-dimensional Raman spectroscopy [7]. However, since we lacked the apparatus required to make such measurements, a simpler and less direct verification of the model was performed. Our approach was to compare predicted temperatures of the reactor outer wall to those measured with a thermocouple. This comparison provides an indirect verification of the model predictions of internal gas temperatures since the outer wall temperatures and internal gas temperatures are interdependent quantities.

Simulations were performed at conditions identical to the experiments. The results of the comparison between the model and the experimental data are shown in Fig. 3. Excellent agreement between the data and the model predictions is demonstrated, indirectly confirming the heat transfer component of the model. Further simulations indicate that the wall temperature is nearly insensitive to susceptor rotation rates of 20 to 500 rpm.

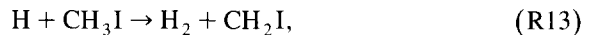
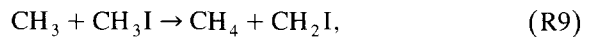
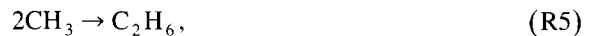
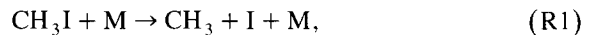
5. CH₃I vapor etching

5.1. Gas phase and surface chemical reactions

A set of elementary reactions that describe the gas decomposition chemistry for CH₃I vapor etching is

based on the assumption that free radicals produced during decomposition are the etchant species. The reaction set includes details about reactions that both produce and consume free radicals, especially I and CH₃.

The thermal decomposition of CH₃I diluted in Ar and other noble gases has been studied in a shock tube over the temperature range 1050–1500 K [8,9]. These are the only known studies to date of the thermal decomposition of CH₃I. Based on the CH₃I decomposition reaction sequence proposed in these earlier studies, the following elementary reaction sequence, which additionally considers reactive effects of a hydrogen carrier, was assembled:



The rate parameters for these reactions are reported in Table 1 and were obtained from several references. The rate parameters for reactions (R10) and (R13) were unavailable in the literature and were estimated by analogy to related hydrogen abstraction reactions from ethane.

A number of calculations were performed using this full set of reactions. However, it was determined that for predicting etch rates from I and/or CH₃ radicals the reduced set of reactions (R1)–(R6) sufficed. It was verified that this reduced reaction set predicted etch rates from I and/or CH₃ radicals

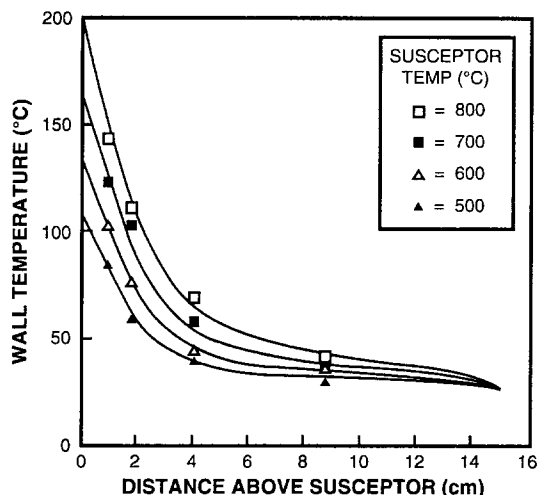
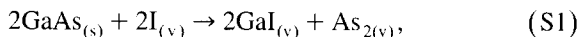


Fig. 3. Wall temperatures predicted by vertical reactor model (solid curves) versus measured wall temperatures (symbols).

within 1% of those predicted from using the full reaction set.

One goal of this modeling work is to test the model for CH_3I vapor etching of GaAs that had been deduced in an earlier study [1], where it had been proposed that free radicals produced by the decomposition of CH_3I in the gas phase react with solid GaAs to form volatile etch products. Examination of the solid etch products which were deposited on the

reactor wall by Auger electron spectroscopy revealed two major deposits, one which primarily contained Ga and I and the other which was primarily elemental As [10]. Gaseous etch products were undetectable by quadrupole mass spectroscopic examination of the exhaust gas from the reactor. The following surface reactions are therefore assumed:



This surface mechanism is consistent with that established for Cl_2 etching of GaAs under high vacuum conditions where for temperatures in excess of 450°C , the etch products are seen to be GaCl and As_2 [15].

5.2. Comparison of model predictions of etch rates with experiments and additional studies

The results of the experimental CH_3I etch studies in the vertical reactor are shown in Figs. 4a and 4b and are compared to etch rates predicted by the model. Generally, for similar etch temperatures and CH_3I mole fractions, etch rates in the vertical reactor were 20–30 times lower than for the same mole fraction of CH_3I in the horizontal reactor operated at atmospheric pressure [1]. These differences can be explained in the context of gas phase decomposition

Table 1

Elementary reactions considered for the decomposition of CH_3I in H_2

No.	Reactants	Products	$\log_{10} A$	E^*/R	B	Ref.
1	$\text{CH}_3\text{I} + \text{M}$	$\text{CH}_3 + \text{I} + \text{M}$	15.4	21439.36	0	[8]
2	$\text{I} + \text{CH}_3\text{I}$	$\text{I}_2 + \text{CH}_3$	14	9964.771	0	[8]
3	$\text{I}_2 + \text{M}$	$2\text{I} + \text{M}$	13.99	15299.45	0	[8]*
4	$2\text{I} + \text{M}$	$\text{I}_2 + \text{M}$			0	
5	2CH_3	C_2H_6	14.1	0	-0.4	[13]
6	$\text{CH}_3 + \text{H}_2$	$\text{CH}_4 + \text{H}$	11.93	5485.657	0	[13]
7	$\text{I} + \text{H}_2$	$\text{HI} + \text{H}$	12.75	16809.26	0	[14]
8	$2\text{H} + \text{M}$	$\text{H}_2 + \text{M}$	17	0	-0.6	[13]
9	$\text{CH}_3 + \text{CH}_3\text{I}$	$\text{CH}_4 + \text{CH}_2\text{I}$	12.5	5083.04	0	[8]
10	$\text{I} + \text{CH}_3\text{I}$	$\text{HI} + \text{CH}_2\text{I}$	13.25	17614.49	0	est.
11	$2\text{CH}_2\text{I}$	$\text{C}_2\text{H}_4\text{I}_2$	14.1	0	-0.4	[8]
12	$\text{H} + \text{HI}$	$\text{H}_2 + \text{I}$	13.7	352.2899	0	[14]
13	$\text{H} + \text{CH}_3\text{I}$	$\text{H}_2 + \text{CH}_2\text{I}$	14.5	6039.255	0	est.
14	$\text{H} + \text{I}_2$	$\text{HI} + \text{I}$	14.6	0	0	[12]

Constants are for rate expression of the form $k = AT^B \exp(-E^*/RT)$.

Rate constants for reactions 10 and 13 were estimated by analogy to related H abstraction reactions from methane taken from Ref. [12].

Rate of reaction 4 is determined from thermodynamics (reverse of reaction 3).

control. The initial decomposition reaction (R1) is pressure dependent and therefore decomposition rates are expected to be roughly 5 times lower because of the lower operating pressure (0.2 atm) of the vertical reactor compared to atmospheric pressure operation of the horizontal reactor system. The CH_3I partial pressure is also 5 times lower in the vertical reactor. For these calculations, the values assumed for σ_{I} and σ_{CH_3} were the largest possible, 1.0, and considering the reaction stoichiometries assumed (S1, S2) these predictions represent upper bound estimates on

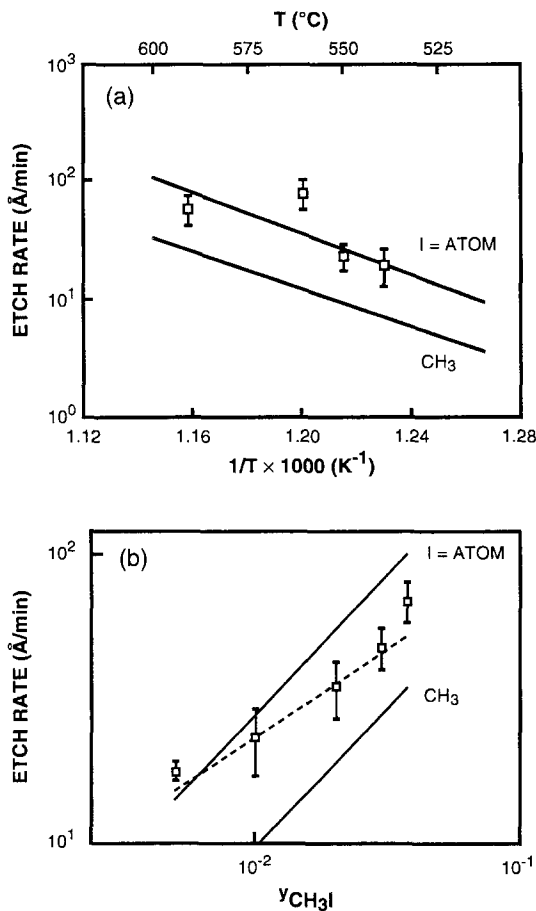


Fig. 4. (a) Predicted temperature dependence of upper bound etch rates in a vertical reactor (solid lines: I atoms and CH_3 radicals) and experimental data (squares w/error bars). Etch conditions: $y_{\text{CH}_3\text{I}} = 0.01$, 10 slpm H_2 , 0.2 atm. Assumed value for σ_{I} , $\sigma_{\text{CH}_3} = 1.0$. (b) Predicted etch rates compared to experimental etch rates in the vertical reactor as a function of CH_3I concentration. Etch conditions: $T = 550^\circ\text{C}$, 0.2 atm, 10 slpm H_2 .

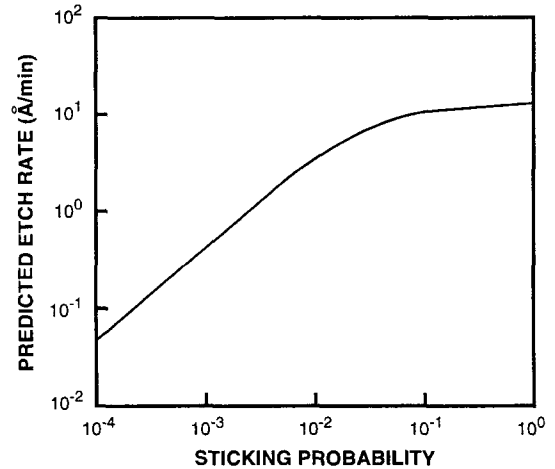


Fig. 5. Predicted etch rate as a function of assumed I sticking probability, σ_{I} . Etch conditions, 525°C , $y_{\text{CH}_3\text{I}} = 0.01$, 10 slpm H_2 , 0.2 atm.

etch rates from these free radical species. As can be seen in Fig. 4, the quantitative agreement between the experimentally measured and predicted etch rates is better for the case of I as the etching species. The predictions for etching by CH_3 are significantly lower than experimental etch rates, ruling out CH_3 radicals as the primary etch species. The error bars shown in Fig. 4 represent errors inherent in the Dektak measurements of etch depth and are relatively large because of the small etched depths ($\sim 1000 \text{ \AA}$ total material removed) compared to the accuracy of the Dektak ($\pm 200 \text{ \AA}$).

The dependence of predicted etch rates on σ_{I} , Fig. 5, shows two distinct regimes. For $\sigma_{\text{I}} > 0.1$, the predicted etch rate is independent of σ_{I} , and the rate is limited by gas phase kinetics. Since a quantitative match between the model predictions and experimental data was found by assuming $\sigma_{\text{I}} = 1.0$, the uncertainty in surface reaction rates is relatively unimportant for the model predictions. At lower values, the predicted rate drops linearly with decreasing σ_{I} , which indicates a mixed surface/gas phase kinetic control regime. These differences are further illustrated in Fig. 6, which shows the structure of the I concentration fields close to the susceptor for two values of σ_{I} . For $\sigma_{\text{I}} = 1.0$, the I concentration contours are observed to turn back in very close to the surface: an internal diffusion boundary layer has

formed very close to the surface and a change in surface reactivity has very little effect on etch rates. At $\sigma_1 = 10^{-5}$, where etch rate is linearly dependent on surface reactivity, the iodine concentration contours terminate at the surface. In both of these cases, gas phase kinetics limit the rate, although at low values of σ_1 surface kinetics are additionally rate limiting. For the discussion that follows, results for both high and low σ_1 values are presented to illustrate differences between these two conditions.

The effect of susceptor rotation rate on etch profiles is shown in Fig. 7 for $\sigma_1 = 10^{-5}$ or 1.0. For both cases, it can be seen that high rotation rates (500 rpm) improve etch rate uniformity across the susceptor from a 30% variation at 20–100 rpm to less than 20% at 500 rpm. The etch rate decreases overall, because of a reduction in thermal boundary layer thickness at high rotation rates, and subsequent reduction in CH_3I decomposition. This result is consistent with previous experimental data for etching in

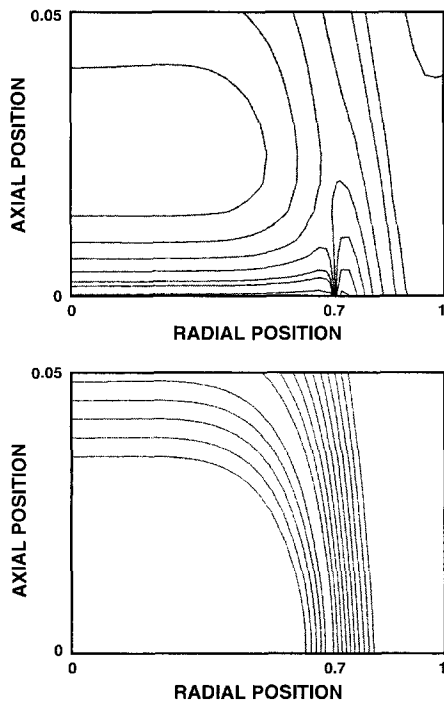


Fig. 6. Structure of I concentration fields for $\sigma_1 = 1.0$ (top) and $\sigma_1 = 10^{-5}$ (bottom). Axial and radial dimensions are normalized to tube radius.

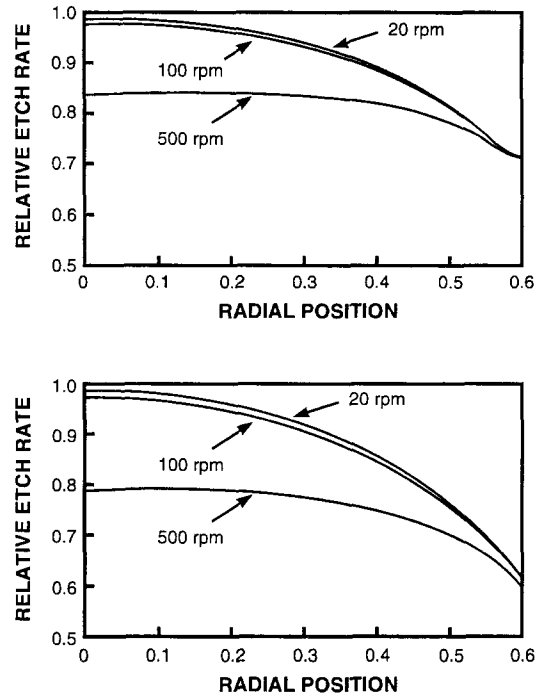


Fig. 7. Predicted effect of disk rotation rate on etch rate and uniformity. Etch conditions: $T = 525^\circ\text{C}$, $\nu_{\text{CH}_3\text{I}} = 0.01$, 10 slpm H_2 , 0.2 atm, $\sigma_1 = 1.0$ (top), $\sigma_1 = 10^{-5}$ (bottom).

a horizontal reactor, where etch rates decreased with increasing flow rate. However, these results are in contrast to previously reported results for the effects of rotation rate on gas phase diffusion-limited growth of GaAs from TMGa and AsH_3 [4], where growth rate increases as rotation rate is increased. In both growth from TMGa and etching from CH_3I , radial uniformity is improved as rotation rate is increased. The fundamental difference between these two scenarios is that TMGa was nearly completely decomposed in the thermal boundary layer, whereas very little CH_3I is consumed in the reaction in the thermal boundary layer. One would expect the results to be more similar if growth experiments were performed at lower temperatures with lower TMGa conversion or if the etching were done at higher temperatures with high conversions of CH_3I .

The sensitivity of etch rate to variations in D_1 and k_1 was also examined. Lennard-Jones parameters for determining I diffusion coefficients could not be found, so the parameters are those previously used

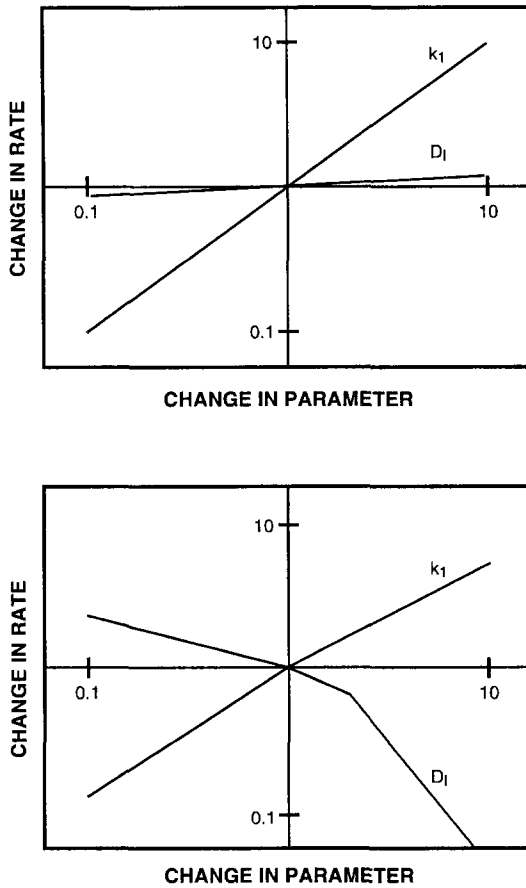


Fig. 8. Sensitivity of predicted etch rates to variations in both k_1 and D_1 . Etch conditions: $T = 525^\circ\text{C}$, $y_{\text{CH}_3\text{I}} = 0.01$, 10 slpm H_2 , 0.2 atm, $\sigma_1 = 1.0$ (top), $\sigma_1 = 10^{-5}$ (bottom).

for diffusion of Ga atoms in H_2 [11]. It is therefore important to check the sensitivity of computed solutions to variations in this diffusivity. The sensitivity of k_1 (R1) was also confirmed to correspond exactly to similar variations in inlet CH_3I concentration. Therefore, the etching reaction order is also reconfirmed by this analysis. The sensitivity to variations in these parameters is illustrated in Fig. 8, which shows the etch rate at the susceptor center as a function of the given parameter value (base value = 1.0) on a log–log plot. Sensitivity is checked for $\sigma_1 = 10^{-5}$ or 1.0, since it is expected that the solution structure is different in the two regimes as shown in Fig. 5.

The results in Fig. 8, to addition to providing a measure of confidence in the computed solution for $\sigma_1 = 1.0$, provide insight to the general nature of a gas phase reaction-limited etching process for conditions of both slow and fast surface reactions. One interesting result is seen for $\sigma_1 = 10^{-5}$, where increasing D_1 results in a decrease in the etch rate. This counter-intuitive result is due to the fact that I atoms are produced within the thermal boundary layer which is itself close to the wafer surface. Therefore, two diffusion processes are occurring simultaneously, diffusion of I to the surface, which leads to etching, and diffusion of I away from the surface due to the fact that the I concentration drops to zero in that direction. For low surface reactivities, the diffusion away from the surface dominates and thus raising D_1 causes a lowering of etch rates. This analysis is confirmed by examining the position and magnitude of the maximum I concentration above the susceptor surface. As is shown in Fig. 6, the maximum is very close to the surface and the concentration gradient at the surface is small. As D_1 is raised, the maximum moves away from the surface but decreases in absolute magnitude, resulting in lower etch rates. In contrast, at high surface reactivities ($\sigma_1 = 1.0$), little dependence of the solution on the assumed value for D_1 is seen and the two competing diffusion processes are in near-perfect balance.

6. Conclusions

A detailed model, which includes $\text{CH}_3\text{I}/\text{H}_2$ multicomponent, multireaction gas phase species conservation with finite surface reactions and radiative heat transfer, was presented for CH_3I vapor etching of GaAs in a vertical rotating-disk reactor. Radiative heat transfer effects were verified by comparison of calculated reactor wall temperatures with experimentally measured values. CH_3I vapor etching of GaAs in the vertical rotating-disk reactor has been examined by considering detailed gas phase reaction chemistry. Comparisons between predicted etch rates and experimentally measured ones support an etching mechanism where I atoms produced by CH_3I gas phase decomposition are the primary etchant species. CH_3 radicals cannot solely account for the experi-

mentally observed etch rates. In general, etch rates in the vertical reactor are much lower than those previously observed in a horizontal atmospheric pressure reactor system because of reduced gas phase decomposition of CH_3I at lower pressures (0.2 atm versus 1 atm). Predictions further show that increasing disk rotation rates leads to improved radial uniformity etch rates. Finally, several observations unique to the gas phase reaction limited nature of this process have been made. Increasing disk rotation rate decreases etch rates, a result which is opposite to what has been observed for gas phase diffusion limited processes. Further, the gas phase reaction limitation acts in series with another limiting process, either surface reactions at low surface reactivities, or gas phase diffusion when the surface reactivity is high.

Acknowledgements

The authors gratefully acknowledge the technical assistance of C.H. Anderson. This work was supported by the National Science Foundation and the Department of the Air Force.

References

- [1] C.W. Krueger, C.A. Wang and M. Flytzani-Stephanopoulos, *Appl. Phys. Lett.* 60 (1992) 1459.
- [2] C.A. Wang, C.W. Krueger, M. Flytzani-Stephanopoulos and R.A. Brown, *J. Electron. Mater.* 21 (1992) 299.
- [3] S. Patnaik, C.A. Wang and R.A. Brown, *J. Crystal Growth* 96 (1989) 153.
- [4] C.A. Wang, S. Patnaik, J.W. Caunt and R.A. Brown, *J. Crystal Growth* 93 (1988) 228.
- [5] W.L. Holstein, *J. Electrochem. Soc.* 133 (1989) 145.
- [6] C.A. Wang, S.H. Groves, S.C. Palmateer, D.W. Weybourne and R.A. Brown, *J. Crystal Growth* 77 (1986) 136.
- [7] D.I. Fotiadis, M. Boekholt, K.F. Jensen and K.F. Richter, *J. Crystal Growth* 100 (1990) 577.
- [8] K. Saito, H. Tahara, O. Kondo and T. Yokubo, *Bull. Chem. Soc. Jpn.* 53 (1980) 1335.
- [9] K. Saito, H. Tahara and I. Murakami, *Bull. Chem. Soc. Jpn.* 57 (1984) 3023.
- [10] C.W. Krueger, PhD Thesis, Massachusetts Institute of Technology (1994).
- [11] A.M. Kremer, MS Thesis, University of Minnesota (1987).
- [12] R.M. Drew, Ed., *CRC Handbook of Bimolecular and Ter-molecular Gas Reactions* (CRC, Boca Raton, Florida, 1987).
- [13] H. Tanaka and J. Komeno, *J. Crystal Growth* 93 (1988) 115.
- [14] J.H. Sullivan, *J. Chem. Phys.* 36 (1962) 1925.
- [15] C. Su, H. Hou, G.H. Lee, Z. Dai, W. Luo, M.F. Vernon and B.E. Bent, *J. Vac. Sci. Technol. B* 11 (1993) 1222.